Journal of Nuclear Materials 571 (2022) 153988

Contents lists available at ScienceDirect

Journal of Nuclear Materials

journal homepage: www.elsevier.com/locate/jnucmat

Ion irradiation induced amorphization of precipitates in Zircaloy

J. Bowman [a], P. Wang [b], G.S. Was [b], M. Bachhav [c], A.T. Motta [a,*]

[a] Ken and Mary Alice Lindquist Department of Nuclear Engineering, The Pennsylvania State University, USA
[b] Nuclear Engineering and Radiological Sciences, University of Michigan, USA
[c] Idaho National Laboratory, USA

ARTICLE INFO

Article history:
Received 5 May 2022
Revised 27 July 2022
Accepted 19 August 2022
Available online 20 August 2022

Keywords:
Zircaloy
Precipitates
Amorphizatoin
Ion irradiation

ABSTRACT

Samples of Zircaloy-4 were ion irradiated at several doses and irradiation temperatures and studied using transmission electron microscopy to discern the amorphization and dissolution behavior of second-phase precipitates under irradiation. It is found that near the critical temperature for amorphization under neutron irradiation a similar amorphization morphology is obtained under proton irradiation as under neutron irradiation, that is, an amorphous layer starting at the precipitate-matrix interface and moving in with increasing dose. However, the rate of amorphous layer advancement is much slower than that seen under neutron irradiation, and saturates with dose so that it remains a partial precipitate amorphization, i.e., this precipitate amorphization mechanism does not lead to complete amorphization as it occurs with neutrons. The results indicate that the critical temperature for bulk amorphization is primarily dependent on the displacement cascade density achievable with the irradiating particle and secondarily with dose rate. Depletion of iron from the precipitates is also observed, although not directly linked to amorphization.

1. Introduction

Zirconium alloy nuclear fuel cladding material behaves differently in the reactor environment than during out-of-reactor testing. In particular, the rates of in-reactor corrosion are higher than those seen during autoclave testing [1]. There are several factors in the reactor environment that can cause this increase. First, corrosion in the reactor occurs under a heat flux and thus, under a temperature gradient which affects cladding stresses, as well as elemental mobility and distribution in the material. Second, the in-reactor chemistry has several additions that can influence corrosion. Finally, and crucially, in-reactor corrosion also occurs under irradiation, which changes the coolant chemistry through radiolysis, and modifies the protective oxide layer and its properties as well as the microstructure and microchemistry of the base metal. These various factors make it difficult to ascribe in-reactor corrosion increases to a specific cause. One approach to address this issue has been to conduct separate effects testing, i.e., designing experiments that investigate each effect individually.

Concerning neutron irradiation induced changes to the base material, such irradiation causes many changes to the as-fabricated nuclear fuel cladding microstructure and microchemistry, including the formation of point defects as well as ⟨a⟩ and ⟨c⟩ dislocation loops, which are associated with matrix hardening and in-reactor deformation such as creep and growth [2–4]. In addition, the distribution of alloying elements may change under irradiation. In the as-fabricated Zircaloy-4, most of the transition metal elements (Fe, Cr) are found in second phase precipitates of the type $Zr(Cr,Fe)_2$ [5,6]. It has been shown by several researchers that changes in the second phase particle size distribution in Zircaloy are associated with significant changes to in-reactor corrosion [7,8]. Thus, it is essential to reproduce the effect of irradiation on the second phase particle composition, size and distribution.

Various researchers have studied the effect of neutron irradiation on second phase particles in Zircaloy [9–11]. Two principal effects have been demonstrated: second phase precipitates become amorphous under irradiation - either homogeneously or heterogeneously - and some of their alloying elements are dissolved into the zirconium matrix either with or without precipitate amorphization, depending on the irradiation temperature [12]. These effects have been observed following high doses under neutron irradiation. Given that neutron irradiation damage rates are low, charged particle irradiation, specifically ion irradiation, has been shown to be a powerful and flexible tool to study irradiation effects in materials, producing many of the same effects as neutron irradiation. However, total dpa doses that take years in reactor can be performed in a few days using self-ion or proton irradiation [13,14] and with little to no residual radioactivity. The precipitates have also been made amorphous by electron irradiation, but this

* Corresponding author.
E-mail address: atm2@psu.edu (A.T. Motta).

https://doi.org/10.1016/j.jnucmat.2022.153988
0022-3115/

Table 1
Sample Irradiation Conditions.

Material	Irradiation Temperature (°C)	Damage (dpa) at 5 μm (proton) and 500–700 nm (Zr^{2+})	Damage Rate (dpa/s) at 5 μm (proton) and 500–700 nm (Zr^{2+})
Zircaloy-4	250 (proton)	1.6	1.65×10^{-5}
	280, 310, 330, 350 (proton)	0.5, 1.6, 5.0	1.65×10^{-5}
	250 (Zr^{2+})	1.6	3.97×10^{-5}

type of irradiation does not produce dense displacement cascades which means that amorphization can only occur at much lower irradiation temperatures than under cascade producing irradiation, as discussed below [15,16]. Also, in order to achieve enough dose electron irradiation has to be much more localized (typically less than 1 μm^2) and is thus not suitable for a post irradiation corrosion experiment.

This project consists of subjecting Zircaloy-4 material to ion irradiation to cause the material microstructure to evolve as it does under neutron irradiation, and to follow this irradiation by corrosion testing. It has been shown that by careful design of the irradiation conditions, proton irradiation of Zircaloy 4 can produce similar dislocation loop size and density, irradiation hardening, precipitate amorphization, and iron redistribution as what is obtained from reactor irradiation [17]. In this paper we focus on the effect of ion irradiation on the amorphization of second phase particles in Zircaloy-4. Samples were irradiated at various temperatures and to a range of doses, and later examined using transmission electron microscopy to ascertain the effect of irradiation. The results are discussed in light of previous work and of current understanding of the amorphization process.

2. Experimental methods

The material used for this experiment was an α-hot-rolled and recrystallization annealed sheet Zircaloy-4 in the form of 2.54 cm by 2.54 cm by 1 mm coupons. The Zircaloy-4 composition was near the average values for alloying and impurity elements outlined in ASTM B811, *Standard Specifications for Wrought Zirconium Alloy Seamless Tubes for Nuclear Fuel Cladding*. Prior to irradiation, 20 mm by 2 mm by 1 mm strips of Zircaloy-4 were machined from these coupons to fit within the irradiation stage at the Michigan Ion Beam Laboratory. Samples were irradiated with a flux of 1.25×10^{14} protons/cm^{2}s at 2 MeV to fluences that resulted in doses of 0.5, 1.6 and 5 dpa at a 5-micron depth, with a constant damage rate of 1.65×10^{-5} dpa/s. Proton irradiations were performed at 250, 280, 310, 330 and 350 °C. One irradiation was performed at 250 °C to 1.6 dpa using 8.1 MeV Zr ions; in that case the target depth for TEM examination was 0.5–0.7 μm. The irradiation temperature was monitored using a 2D FLIR Thermal Imaging System at multiple locations for each irradiation throughout the experiment. The FLIR thermal imager was calibrated to the reading obtained from the j-type thermocouples pre-welded to the samples. The list of conditions used for irradiation of the alloy in this study is given in Table 1. Note that taking samples from other depths in the foil than at the target depths given in Table 1 can yield different doses, albeit at different dose rates. A detailed description of the irradiation stage and resulting microstructures is provided in ref. [17].

This specific set of irradiation temperatures was selected to study the critical temperature for amorphization of the $Zr(Cr,Fe)_2$ second phase particles [18]. The specific energy of 2 MeV protons was selected for the combined purposes of attaining an appropriate penetration depth (>25 μm), a reasonably flat profile up to a depth of approximately 20 μm, and a sufficiently high damage rate to achieve a few dpa in a reasonable time. The damage levels are calculated using the Stopping and Range of Ions in Matter (SRIM) software using a K-P model and a displacement energy of 40 eV. An example output of this software for the 5 dpa irradiated samples is provided in Fig. 2. The SRIM damage profile shows the predicted damage level as a function of depth. Clearly, because the displacement rates are different, the dose rates at the different depths also vary by up to an order of magnitude, so that this dose rate effect on amorphization is thought to be small [19].

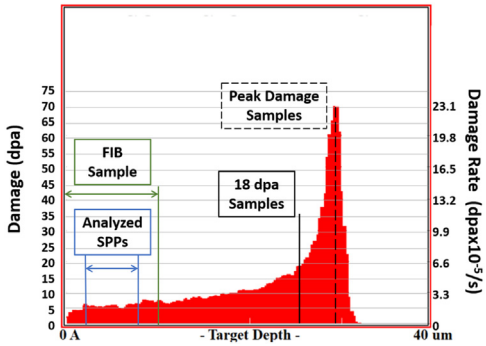

Fig. 1. Damage Profile in Zircaloy sample irradiated with 2 MeV protons to a fluence of 7.8 × 10^{19} protons/cm^2. This corresponds to a level of damage of 5 dpa at 5 μm depth. The depth from which the 18 dpa sample was extracted is also shown.

The focused ion beam milling (FIB) lift-out method was used to extract cross sectional samples that were approximately 10 μm wide and 6 μm tall and between 50 and 100 nm thick. The steps used to prepare the sample are shown in Fig. 2, and include: a) carbon deposition using 5 keV electrons and 30 keV gallium ions, b) milling large chunks using 30 keV gallium ions, c) milling a J-shaped cut to prepare for extraction, d) attaching the lamella to a TEM grid, and e) final thinning of the sample. These steps were performed at varying currents and temperatures in order to minimize hydride formation, gallium implantation, and to avoid sample bending. This depth location from the sample surface afforded by FIB was better than 0.5 μm. For each irradiation condition multiple foils were extracted. The samples at 18 and 70 dpa were taken from different depths in the sample.

The TEM samples were examined using bright-field imaging, diffraction analysis, and energy dispersive spectroscopy in a FEI Talos F200X at both Penn State and at the University of Michigan. Bright-field images showed the presence of amorphous rims on precipitates, indicated by a region of differing contrast near the outer surface of the precipitate. Bright-field imaging can confirm crystallinity of a region through the presence of stacking faults in the crystalline portion of the precipitates and can be used to determine precipitate morphology. Diffraction pattern analysis enabled the determination of the crystalline structure of the SPPs and confirmed bright-field observations as to whether a region was crystalline or amorphous. Energy dispersive spectroscopy was used to quantify the composition of SPPs in order to monitor overall chemical changes and specifically to track changes in iron content.

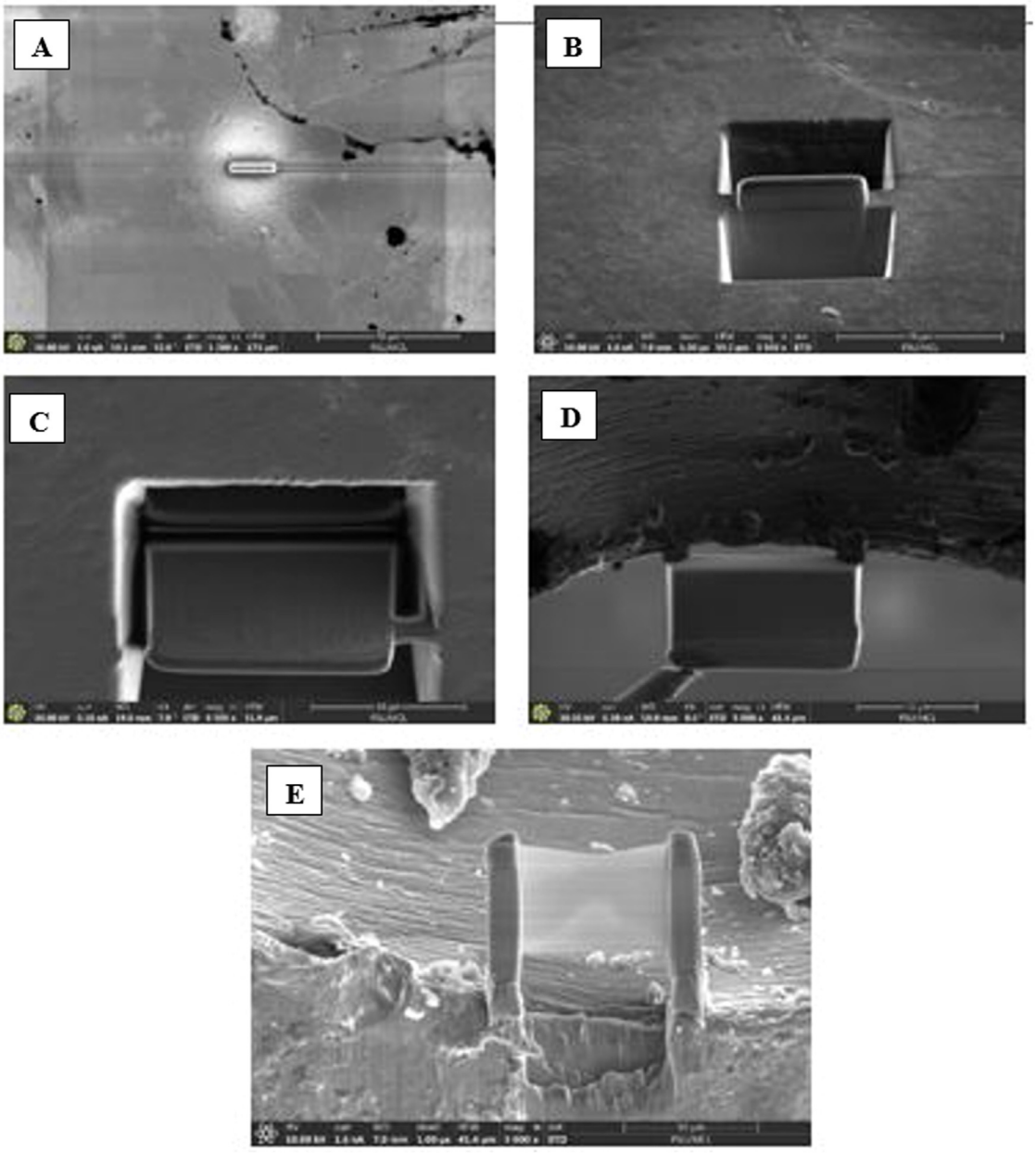

Fig. 2. FIB Sample Preparation Images of Protective Carbon Deposition (A), Milling (B), J-Shaped Cut (C), Attachment to Extraction Probe (D), and Final Thinning on TEM Grid (E).

3. Results

This section presents the experimental results of the ion irradiations conducted in this study on the irradiation-induced crystalline-to-amorphous transformation (amorphization) of $Zr(Cr,Fe)_2$ precipitates in Zircaloy 4.

3.1. Amorphization of $Zr(Cr,Fe)_2$ precipitates

Fig. 3 shows a precipitate particle after 2 MeV proton irradiation at 280 °C. At the sample depth from which this sample was prepared the dose was 18 dpa. After this dose the precipitate exhibited a similar morphology to that seen under neutron irradiation when irradiated close to the neutron irradiation critical temperature, that is, an amorphous rim and a crystalline interior [2]. In this case the rim was measured to be 22 nm thick in a roughly 100 nm diameter precipitate, as indicated. The crystalline precipitate showed the characteristic stacking faults seen in $Zr(Cr, Fe)_2$ Laves phase precipitates [20]. In this case a diffraction pattern for this precipitate was obtained which could be indexed as C14 hcp $MgCu_2$ type Laves phase, in agreement with previous observations [21,22].

Several irradiations at a range of temperatures to various doses were performed in this study, followed by transmission electron microscopy examination of the irradiated microstructures. The thickness of the amorphous layer was measured after irradiation at various temperatures and the result is shown in Fig. 4. Although similarly to what was seen under neutron irradiation in LWR conditions, the thickness of the amorphous rim increased with dose, the increase was substantially lower, on a per dpa basis, than that

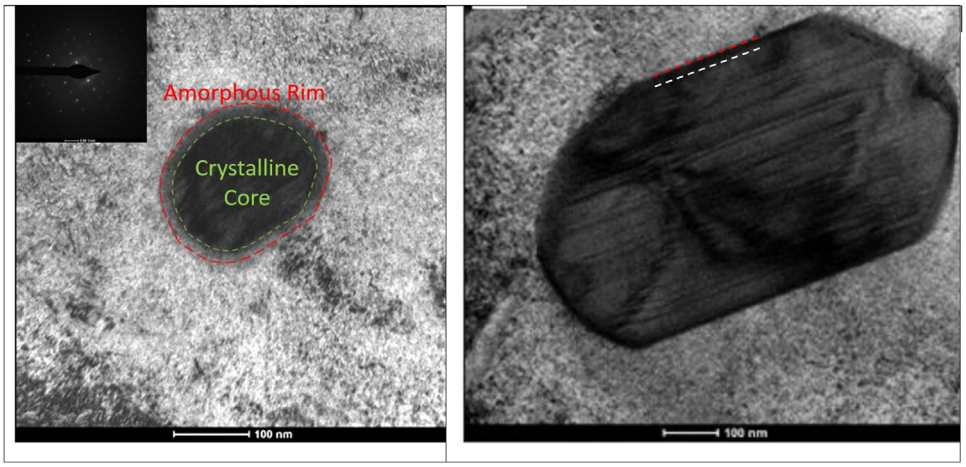

Fig. 3. $Zr(Cr,Fe)_2$ precipitate in Zircaloy after irradiation with 2 MeV protons (a) to 18 dpa at 280 °C, (b) to 5 dpa at 310 C.

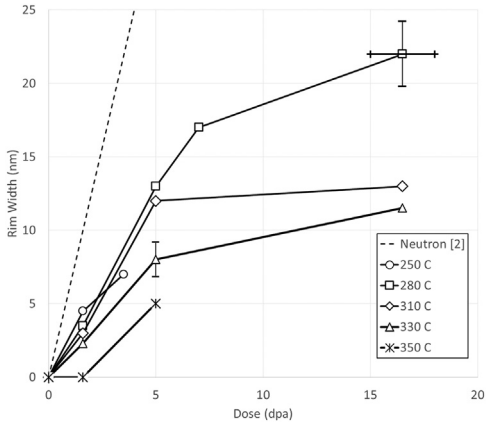

Fig. 4. Amorphous Rim thickness of $Zr(Cr,Fe)_2$ precipitates versus dose at various irradiation temperatures for proton and neutron irradiation. Typical error bars for width and dose are shown. The dose bars at the highest dose are the largest because of the increase in dpa at that depth.

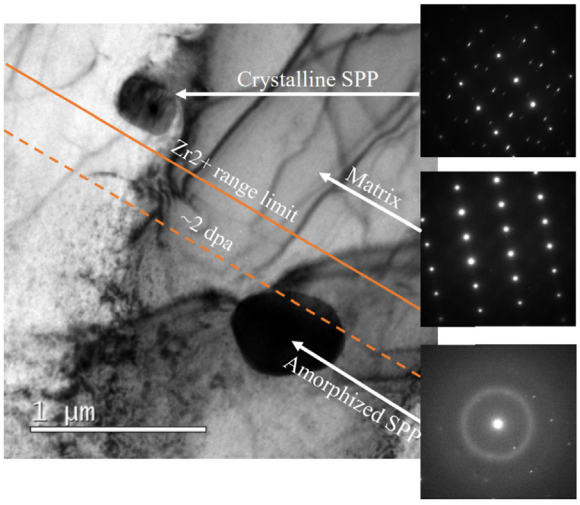

Fig. 5. $Zr(Cr,Fe)_2$ precipitates in Zircaloy after irradiation with 8.1 MeV Zr^{2+} ions at 250 °C.

seen under neutron irradiation. The growth of the amorphous rim with dose decreased with increasing irradiation temperature for a given dose.

The measured amorphous rim thicknesses are plotted versus irradiation dose in Fig. 4, where they are also compared with the previously reported value for the amorphous rim thickness under neutron irradiation (dashed line) [2]. We do note that the rim thickness measurement involves some uncertainty of at least a few nm – the representative error bar shown is related to the percent uncertainty in the measurement of the rim about +/- 12% and scales with the rim thickness. We note however, that the exact value of the amorphous layer thickness is not thought to be that important, but, rather, the fact that amorphization does not proceed in the same manner as under neutron irradiation. Indeed, it can be noticed that, in contrast with neutron irradiation which shows a constant rate of advancement of the amorphous layer throughout the process, the rate of advancement of the amorphous layer under proton irradiation decreases with dose, possibly indicating a tendency to saturate. Thus, the amorphization shown here is only partial amorphization and will not proceed to the whole precipitate.

Irradiation with Zr ions conducted at a much lower irradiation temperature (250 °C) quickly resulted in complete precipitate amorphization, as shown in Fig. 5. The region in Fig. 5 where the amorphous precipitate was seen received a total dose of approximately 2 dpa. It could not be ascertained whether amorphization started at the rim and progressed in, as the precipitate was completely amorphous when examined. Finally irradiation with protons at a temperature of −10 °C to 2.5 dpa resulted in complete amorphization. The fact that under proton irradiation only incomplete amorphization was observed even at 250 °C, leads us to believe that the critical temperature for amorphization under proton irradiation is between room temperature and 250 °C, likely because the cascade density that can be achieved under proton irradiation is lower than what can be achieved under heavy ion or neutron irradiation, as discussed below.

3.2. Microchemical evolution

In addition to the morphological changes related to loss of crystallinity, microchemical changes in the precipitates were also observed after irradiation. In the neutron irradiated case, depletion of primarily Fe (and to a lesser extent of Cr) from the amorphous rim was seen. This was not clearly observed under proton irradiation to similar doses. Although an amorphous layer was seen in the proton irradiated samples in this study, no systematic loss of Fe specific to the amorphous layer was observed, as measured by

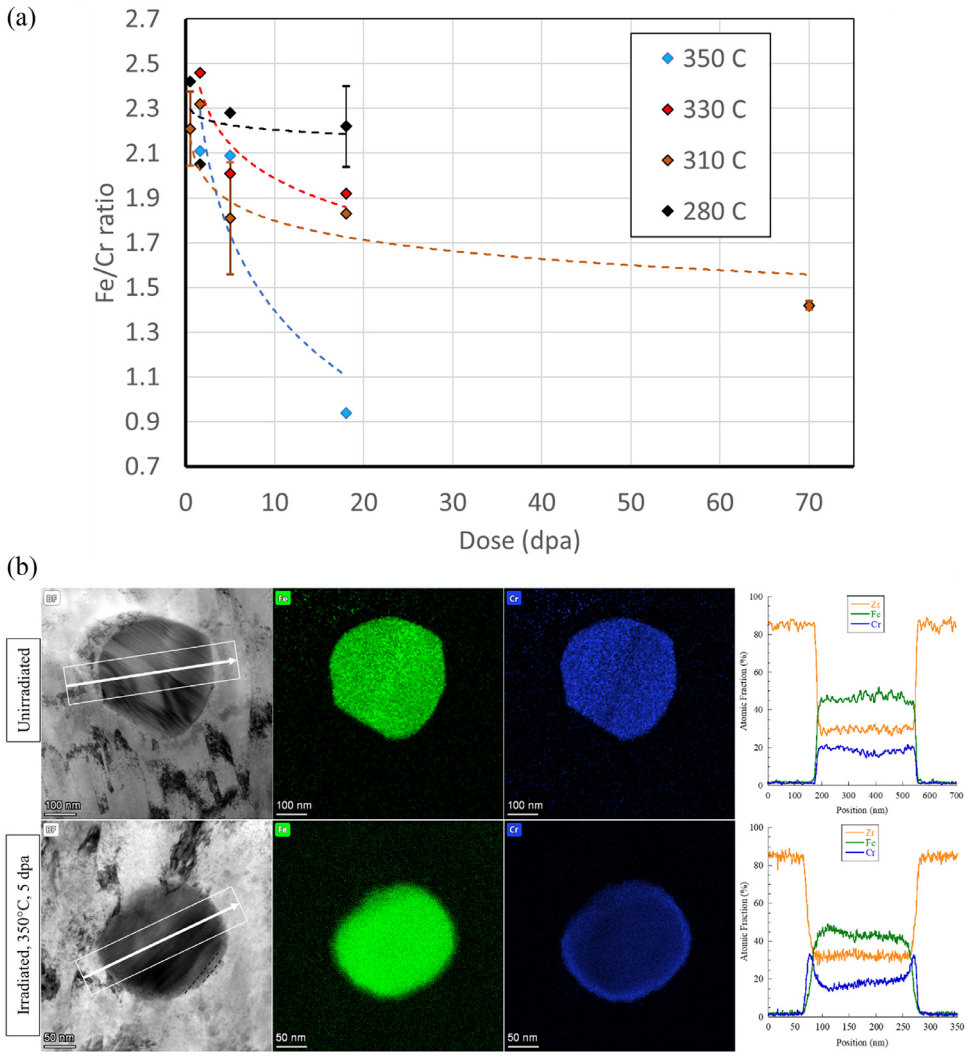

Fig. 6. (a) Fe/Cr ratio of $Zr(Cr,Fe)_2$ precipitates versus dose at various irradiation temperatures for proton irradiation - the 310 °C data shows a fit to guide the eye (b)Bright-field transmission electron micrographs and elemental maps of $Zr(Cr,Fe)_2$ precipitates in two conditions: unirradiated and proton irradiated (350 °C, 5 dpa); compositional maps for the same and line scans across the region indicated showing Zr, Cr and Fe.

EDS (this may also be a result of the small amorphous rim thickness in relation to the volume examined by the electron beam). It should be mentioned that the examination of one of the atom probe needles [17] showed a loss of Fe in a region similar to that seen in neutron irradiation the amorphous layer, but as this phenomenon was not observed systematically, the issue is yet to be resolved.

An o verall decrease in the Fe/Cr ratio occurred as a result of irradiation, but over the bulk of the precipitate, including the part that was not amorphous. The initial Fe/Cr ratio in the alloy was ~ 2.5, similar to the overall composition of the alloy [24]. As measured by Energy Dispersive Spectroscopy (EDS), both the Fe/Cr and (Fe+Cr)/Zr ratios were lower in irradiated precipitates than in non-irradiated ones. Fig. 6 shows EDS measurements of the Fe/Cr ratio performed on several precipitates, as a function of dose for several irradiation temperatures. Significant decreases in the Fe/Cr ratio are seen at all conditions studied. The decreases occurred homogeneously throughout the precipitates, and in particular are not associated with the amorphous layer, as was observed under neutron irradiation [11]. The decrease in Fe is more marked at higher irradiation temperatures and is not linked to precipitate amorphization, which actually becomes more difficult as the temperature increases, as noted above. Rather, the overall Fe/Cr ratio in the whole precipitate decreased with dose, whether or not amorphization occurred. From the data in 6a and assuming the Cr content in the precipitate stays the same after irradiation, the degree of Fe loss was significant. => please see new Figure 6a attached to the email message

Even discounting the point at (18 dpa, 350 ° C), the decrease in Fe/Cr ratio is marked: for example, the ratio does fall below 2 at 310 °C. Note further that one sample was taken at the peak of the damage (70 dpa) for the sample at 310 C, and shows a decreasing Fe/Cr ratio. A trend curve is drawn to illustrate. This is especially true near the precipitate edge. It is not clear, given such a large departure from stoichiometry, why the precipitates remain crystalline, as this change would entail either a high concentration of antisite defects or a large degree of chemical disorder. Fig. 6b shows a comparison of the precipitate composition in two states: unirradiated and a proton irradiated (5 dpa, 350 °C). In the irradiated precipitate although no Fe plateau is seen at the periphery, the Cr content is very much increased, suggesting that some Fe has left the precipitate. Calculating the slope of the Fe/Cr ratio at the edge of the precipitate also shows that the slope decreases with dose, further indicating Fe loss.

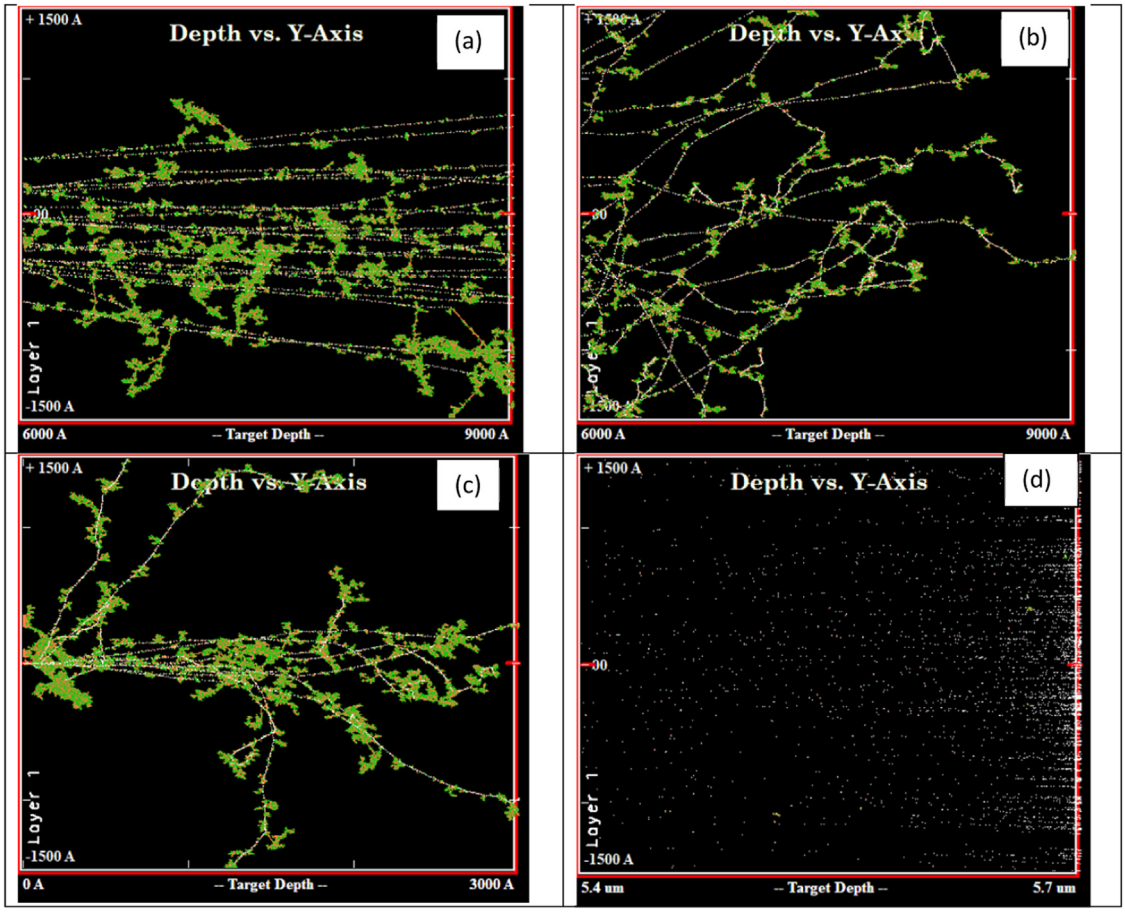

Fig. 7. Monte Carlo Simulations of cascades in Zr using (a) 20 keV Zr ions, (b) 600 keV Ne ions, (c) 350 keV Ar ions and (d) 2 MeV protons.

4. Discussion

Amorphization in intermetallic compounds occurs when enough damage accumulates in the microstructure to make it energetically favorable for the ordered material to give up its long-range topological order in order to maintain short-range chemical order [18]. The irradiation damage causes crystalline phases. That is:

$$\Delta G_{irr} \geq \Delta G_{C-A} \tag{1}$$

where $\Delta G_{irr}$is the Gibbs energy increase brought about by irradiation and $\Delta G_{C-A}$is the Gibbs energy difference between the crystalline and amorphous phases [23].

$$\Delta G_{irr} = \sum_j C_j E_j \tag{2}$$

Where C is the defect concentration, and E is the defect energy and the subscript j stands for the different defects present (single defects, clusters). This free energy increase can only occur if irradiation is performed under the critical temperature for amorphization so that irradiation damage in the form of defects and chemical energy can accumulate in the precipitate faster than thermal annealing can eliminate them [24]. Above the critical temperature for amorphization the annealing rate is greater than the defect production rate, so not enough damage accumulates and amorphization does not occur.

We note that the amorphization process of $Zr(Cr,Fe)_2$ precipitates under ion irradiation was also investigated with two other studies, both performed in situ, i.e. by irradiating electron thin foils with ions while observing the process in the TEM. The first study used 350 keV Ar ions to a dose of 20×10^{16} (ion/cm^2) at a range of temperatures from 27 to 377 °C, corresponding to about 130 dpa [25]. The critical temperature for amorphization was found to be near 377 °C. The irradiation temperature at which amorphization was still achieved was considerably higher than that in proton irradiation, likely because of the denser cascades achievable with Ar ions. The second study used 600 keV Ne ions at 350 °C which produced complete amorphization after 1.2 dpa. In both thin foil irradiations, amorphization proceeded in a different manner than in bulk ion or neutron irradiation, in that the entire precipitate became amorphous gradually and homogeneously, i.e. without starting from the rim. This is likely caused by the fact that thin foils have a precipitate-matrix interface that is only as thick as the thickness of the foil, thus reducing the role of the interface in causing amorphization. A previous study of proton irradiation of $Zr(Cr,Fe)_2$ precipitates in Zircaloy also showed preferential amorphization at the precipitate matrix interface: a 10 nm thick amorphous layer was observed after irradiation to 5 dpa at 310 °C [26]. That is, the amorphization morphology was similar to that seen under neutron irradiation, but with a lower rate of advancement of the amorphous layer. The amorphous thickness reported corresponds to the amorphous thickness measured in this study at 5 dpa, but at a lower irradiation temperature, 280 °C.

Thus, we make a clear distinction between partial and bulk amorphization. The discussion on critical temperature for amorphization refers to the latter. The critical temperature for bulk amorphization under electron irradiation of these precipitates is near room temperature (27 °C) [15] while for neutron irradiation it is between 288 and 310 °C [24]. This large difference between electrons and neutrons is likely caused by the fact that electron ir-

radiation produces isolated defects, rather than defect clusters. This occurs because the recoil spectrum achieved under high energy electron irradiation is much lower in energy than can be achieved by irradiations that can create dense displacement cascades such as neutron irradiation (i.e. the primary knock on atom (PKA) energies are much lower in electron irradiation). We further note that a range of recoil spectra can be achieved for different ions, depending on the ion/target mass and ion energy. In particular, the displacement cascades obtained with self-ion irradiation are most similar to those seen under neutron irradiation[1], and those have the highest possible cascade densities, as the energy transfer parameter is maximized. In contrast, cascade densities achieved with proton irradiation are much lower.

At low temperature no concurrent annealing is present during irradiation so that irradiation induced amorphization happens homogeneously. As the irradiation temperature increases, the annealing rate also increases, and eventually causes the damage accumulation to decrease to zero. The temperature at which this occurs is the critical temperature for amorphization. From the above discussion, it is clear that the critical temperature for amorphization depends on how dense the displacement cascades are. In other words, annealing of isolated defects can occur at near room temperature, while annealing of the more complex defect clusters produced by the dense damage cascades in neutron irradiation occurs near reactor temperature.

Although it is difficult to quantitatively estimate cascade density, it is possible to obtain a qualitative idea of the difference between irradiations by running the SRIM code for different irradiating particles. The simulations were run in Zr using SRIM 2008 in full cascade mode, with a displacement energy of 25 eV. In each case a 300 nm window is shown for comparison, near the depth where the TEM examination was conducted in each case. Fig. 7(a) shows 20 keV Zr, (b) shows 600 keV Ne [26], [c] shows 350 keV Ar [25] and (d) shows 2 MeV protons. It is clear that dense cascades form in (a-c) while (d) shows mostly isolated defects. Since isolated defects are easier to anneal, the critical temperature for amorphization under proton irradiation is likely lower than under heavy ion irradiation.

A couple additional mechanisms can extend the critical temperature for amorphization: departure from stoichiometry at the interface [2] and a higher dose rate [19]. Under neutron irradiation at reactor operating temperatures, precipitate amorphization starts on the outer rim of the particle, near the precipitate-matrix interface and advances in until the particle is completely amorphous [2]. The advance of the amorphous layer occurs at a roughly constant rate of 10 nm/10^{25} m^{-2} or about 5 nm per dpa [2]. In parallel with amorphization a loss of iron from the precipitate is observed, dropping the iron content from 40 at% in the crystalline particle to ~10% in the amorphous layer. Both effects have been explained as the result of additional ballistic mixing near the precipitate interface and change in precipitate-matrix equilibrium induced by amorphization [27]. Such mixing increases the precipitate free energy near the precipitate matrix interface, (relative to the precipitate center), causing amorphization to start at the precipitate edge. This additional change near the precipitate rim favors amorphization at that location.

On the other hand, while neutron and proton irradiation cause amorphization of $Zr(Fe,Cr)_2$ particles at considerably higher temperatures than electron irradiation due to the larger cascades size produced by both, amorphization at the precipitate periphery appears to be possible at a slightly higher temperature with proton irradiation than with neutron irradiation despite the smaller cascade size produced by protons.[2] However, the dose rate with proton irradiation in this study is two to three orders of magnitude higher than occurs under neutron irradiation in an LWR. It has been shown that a higher dose rate can lead to a higher critical amorphization temperature. This idea is also quantified in Mansur's temperature shift idea for corresponding microstructures between ion and neutron irradiation [28].

In summary, amorphization can occur when the damage rate is higher than the annealing rate. Since the annealing rate increases with temperature, at a high enough temperature (above the critical temperature) no amorphization is possible. The critical temperature for annealing the defects whose accumulation can lead to amorphization is primarily dependent on the cascade density, and increases with cascade density, since denser cascades produce larger defect clusters that are more difficult to anneal than isolated defects. Although a higher damage rate competes with diffusional annealing, the exponential dependence of the latter can more easily overwhelm the higher damage rate, thus extending the critical temperature only to a limited extent. A departure from stoichiometry (possible near the edge of second phase precipitates) can extend that temperature to somewhat higher values.

5. Conclusions

A detailed set of ion irradiations at temperatures between 250 and 350 °C and doses up to 70 dpa has been performed on second phase $Zr(Cr,Fe)_2$ precipitates in Zircaloy-4. The main conclusions are as follows:

1. Amorphization of $Zr(Cr,Fe)_2$ precipitates in Zircaloy-4 can be induced by ion irradiation. In the low temperature range, amorphization occurs homogeneously, while at high temperature amorphization occurs preferentially at the precipitate matrix interface. However, contrary to neutron irradiation this only results in partial amorphization.
2. The critical temperature for *bulk* amorphization, (above which amorphization under irradiation is no longer possible) increases with the achievable cascade density for the particular irradiation type. Thus, for a fixed damage rate, the critical temperature for bulk amorphization is lowest for electron irradiation, followed by amorphization under proton irradiation, and under self-ion and neutron irradiation.
3. Significant depletion of iron from the $Zr(Cr,Fe)_2$ was seen after irradiation, but it was not related to the occurrence of amorphization. In particular, the amorphous layers formed were not systematically depleted in iron and conversely, iron depletion occurred even during one of the 350 °C irradiations in which no amorphization occurred.

Data availability

Data will be made available on request.

Declaration of Competing Interest

The authors declare that they have no known competing financial interests or personal relationships that could have appeared to influence the work reported in this paper.

Acknowledgments

This work was supported through the INL Laboratory Directed Research & Development (LDRD) Program under DOE Idaho Opera-

[1] Neutron irradiation essentially produces a recoil spectrum of self ions.

[2] We do note that it is possible that a higher flux neutron irradiation may increase the neutron irradiation critical temperature somewhat.

tions Office Contract DE-AC07–05ID14517, under the MUZIC program. The authors acknowledge the support of the staff of the Michigan Ion Beam Laboratory for the ion irradiations.

References

[1] A.T. Motta, A. Couet, R.J. Comstock, Corrosion of Zirconium Alloys Used for Nuclear Fuel Cladding, Annu. Rev. Mater. Res. 45 (2015) 311–343.

[2] M. Griffiths, Review of microstructure evolution in zirconium alloys during irradiation, J. Nucl. Mater. 159 (1988) 190–218.

[3] F. Christien, A. Barbu, Effect of self-interstitial diffusion anisotropy in electron-irradiated zirconium: a cluster dynamics modeling, J. Nucl. Mater. 346 (2005) 272–281.

[4] R.B. Adamson, C.E. Coleman, M. Griffiths, Irradiation creep and growth of zirconium alloys: a critical review, J. Nucl. Mater. 521 (2019) 167–244.

[5] C. Lemaignan and A.T. Motta, "Zirconium Alloys in Nuclear Applications," in *Materials Science and Technology, A Comprehensive Treatment*. vol. 10 B, B. R. T. Frost, Ed., ed New York: VCH, 1994, pp. 1–51.

[6] S. Kass, The Development of the Zircaloys, in: Symposium on Corrosion of Zirconium Alloys, ANS Winter meeting, 1963, STP 368, New York, 1964, pp. 3–27.

[7] IAEAWaterside Corrosion of Zirconium Alloys in Nuclear Power Plants, International Atomic Energy Agency, Vienna IAEA-TECDOC-996, 1998.

[8] IAEA, Corrosion of Zirconium Alloys in Nuclear Power Plants, IAEA (1993) Vienna IAEA-TECDOC-684.

[9] F. Garzarolli, W. Goll, A. Seibold, I. Ray, Effect on In-PWR Irradiation on Size, Structure and Composition of Intermetallic Precipitates of Zr Alloys, in: *11th International Symposium on Zr in the Nuclear Industry*, STP 1295, 1996, pp. 541–556.

[10] R.W. Gilbert, M. Griffiths, G.J.C. Carpenter, J. Nucl. Mater. 135 (1985) 265–268.

[11] W.J.S. Yang, R.P. Tucker, B. Cheng, R.B. Adamson, J. Nucl. Mater. 138 (1986) 185–195.

[12] D. Gilbon, C. Simonot, Effect of Irradiation on the Microstructure of Zircaloy-4, in: *10th International Symposium on Zr in the Nuclear Industry*, STP 1245, Baltimore, MD, 1994, pp. 521–548.

[13] G.S. Was and R.S. Averback, "1.07 - Radiation Damage Using Ion Beams," in *Comprehensive Nuclear Materials*, R. J. M. Konings, Ed., ed Oxford: Elsevier, 2012, pp. 195–221.

[14] A. Harte, T. Seymour, E.M. Francis, P. Frankel, S.P. Thompson, D. Jadernas, Advances in synchrotron x-ray diffraction and transmission electron microscopy techniques for the investigation of microstructure evolution in proton- and neutron-irradiated zirconium alloys, J. Mater. Res. 30 (2015) 1349–1365.

[15] A.T. Motta, D.R. Olander, Theory of Amorphization Under Electron Irradiation, Acta Metall. Mater. 38 (1990) 2175–2185.

[16] A.T. Motta, D.R. Olander, A.J. Machiels, Electron-Irradiation Induced Amorphization of Precipitates in Zircaloy-2, in: *14th International Symposium on Effects of Radiation on Materials*, STP 1046, Andover, Ma, 1989, pp. 457–469.

[17] P. Wang, J. Bowman, M. Bachhav, B. Kammenzind, R. Smith, J. Carter, Emulation of Neutron Damage with Proton Irradiation and Its Effects on Microstructure and Microchemistry of Zircaloy-4, J. Nucl. Mater. 557 (2021) 153281.

[18] A.T. Motta, Amorphization of Intermetallic Compounds under Irradiation-a Review, J. Nucl. Mater. 244 (1997) 227–250.

[19] A.T. Motta, L.M. Howe, P.R. Okamoto, Amorphization of Zr3Fe under electron irradiation, J. Nucl. Mater. 270 (1999) 174–186.

[20] L.M. Howe, D. Phillips, A.T. Motta, P.R. Okamoto, Irradiation induced phase transformation in zirconium alloys, Surf. Coat. Technol. 66 (1994) 411–418.

[21] D. Arias, J.P. Abriata, The Fe-Zr (Iron-Zirconium) System, Bull. Alloy Phase Diagrams 9 (1988) 597–604.

[22] P. Vizcaíno, A.D. Banchik, J.P. Abriata, Synchrotron X-ray diffraction evidences of the amorphization/dissolution of the second phase particles (SPPs) in neutron irradiated Zircaloy-4, Mater. Lett. 62 (2008) 491–493 2008/02/15/.

[23] W.J. Weber, R.C. Ewing, C.R.A. Catlow, T. Diaz de la Rubia, L.W. Hobbs, C. Kinoshita, Radiation Effect in Crystalline Ceramic Phases Relevant to the Immobilization and disposition of Nuclear Waste and Weapons Plutonium, J. Mater. Res. 13 (6) (1998) 1434–1484.

[24] A.T. Motta, F. Lefebvre, C. Lemaignan, Amorphization of precipitates in Zircaloy under neutron and charged-particle irradiation, in: 9th International Symposium on Zirconium in the Nuclear Industry, ASTM Special Technical Publication 1132, 1991, pp. 718–737.

[25] A.T. Motta, L.M. Howe, P.R. Okamoto, Amorphization kinetics of Zr (Cr, Fe)2 under ion irradiation, in: Materials Research Society Symposium Proceedings: Beam Solid Interactions: Fundamentals and Applications, 279, Boston, MA, USA, 1993, pp. 517–522.

[26] X.T. Zu, K. Sun, M. Atzmon, L.M. Wang, L.P. You, F.R. Wan, Effect of proton and Ne irradiation on the microstructure of Zircaloy 4, Philos. Mag. 85 (2005) 649–659.

[27] A.T. Motta, C. Lemaignan, A Ballistic Mixing Model for the Amorphization of Precipitates in Zircaloy, J. Nucl. Mater. 195 (1992) 277–285.

[28] E.H. Lee, L.K. Mansur, Unified theoretical analysis of experimental swelling data for irradiated austenitic and ferritic/martensitic alloys, Metal. Trans. A (Phys. Metal. Mater. Sci.) 21A (1990) 1021–1035.